reference image and forward-projected, and the reconstruction matrix is large enough to contain the whole object;

Step3: Truncated data from small FOV detector are used as real projection in the MLEM reconstruction process.

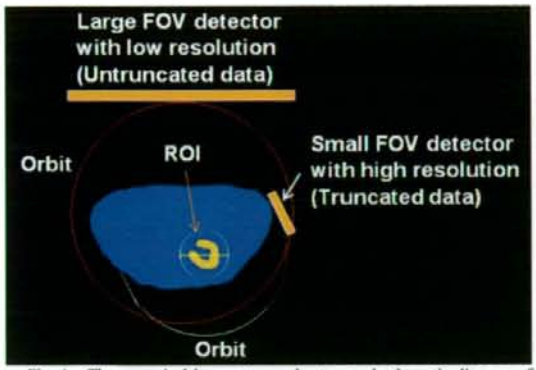

Fig. 1. The numerical human torso phantom and schematic diagram of SPECT system with two kinds of detectors. Untruncated data from low-resolution detector with large FOV are used to compensate the artifact and overestimation due to truncation in small FOV detector. The white line shows the small FOV detector and its circular orbit over 180° to image heart with high resolution. The red line shows the large FOV detector and its circular orbit over 360° to acquire untruncated projection data.

B. Computer Simulation

This simulation was performed using the numerical human torso phantom as shown in Fig. 1. Image matrix is 256 pixels × 320 pixels. Assuming pixel size of 1.14 mm, image size 360 mm × 290 mm. Pixel values are 3 and 1 for heart and the surrounding area.

The small FOV detector with high resolution has 1.14-mm resolution, 80-mm FOV and parallel collimator. The whole of heart was included in this FOV, but the surrounding area was truncated. Projection data of ROI shown by white circle in Fig. 1 were acquired by a circular orbit shown by white line, over 180°, with 3°step and 60 views. The large FOV detector with low resolution has 9-mm resolution, 360-mm FOV and parallel collimator like conventional clinical SPECT. The projections data including the whole of thorax were acquired without truncation by this large FOV detector. A red circle in Fig. 1 shows orbit of the large FOV detector. Projection data were acquired with 3° step and 120 views over 360°. Gaussian noises were added to all projection data. Data from the small FOV detector were reconstructed by MLEM method as iterative reconstruction method, on the reconstruction matrix of 256 pixels ×320 pixels large enough to contain the whole of thorax. The reconstructed image from the large FOV detector was used as an initial image in iterative reconstruction. To compare with conventional reconstruction method, projection data with 70 bins were reconstructed on the reconstruction matrix of 70 pixels ×70 pixels. The number of iteration in MLEM reconstruction was 16.

To compare with conventional clinical SPECT, untruncated projection data including the whole of the brain were acquired by a 360-mm FOV (40 bin) detector with low resolution of 9 mm, over 360°, with 3° step and 120 views. After adding Gaussian noise, the projection data were reconstructed by OSEM method as one of iterative reconstruction method, with 8 subsets and 2 iterations.

As reference image, untruncated projection data including the whole of the brain were acquired by a 360-mm FOV (320 bin) detector with high resolution of 1.14 mm, over 360°, with 3° step and 120 views. After adding Gaussian noise, the projection data were reconstructed by OSEM method as one of iterative reconstruction method, with 8 subsets and 2 iterations. However, this detector is impractical because it is too expensive if manufactured.

The images obtained in this simulation were visually compared, and also the profiles of the images were obtained on straight line over heart shown in Fig. 1 to compare quantitatively.

In this simulation, the effects of attenuation, scatter and blurring by collimator were not considered because this simulation was aimed at evaluating truncation-compensated method.

Furthermore, we evaluated the rotating angle in the orbit of small FOV detector. Small rotating angle is desirable because the detector can be closer to the object when the rotating angle is smaller as shown in Fig. 2. Therefore, the small rotating angle improves the sensitivity and the resolution. The rotating angles of 45 °, 90°, 120°, 150° and 180° were tested. All projection data were reconstructed by our proposed method.

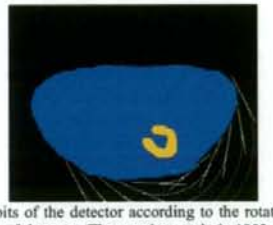

Fig. 2. The orbits of the detector according to the rotating angles. White lines are the orbits of detector. The rotating angle is 180° for the outermost orbit. The rotating angle is 45° for the innermost orbit.

III. Results and Discussion

Figure 3(a) shows the image reconstructed from untruncated projection data using the small FOV detector with low resolution. The obtained image had low resolution. The heart was blurred.

Figure 3(b) shows the image reconstructed from untruncated projection data using the large FOV detector with high resolution. The clear image with high resolution was obtained. However, such a high resolution and large FOV detector is impractical because it is too expensive if manufactured.

Figure 3(c) shows the image reconstructed from truncated projection data obtained using the small FOV detector with high resolution. The projection data were reconstructed on the small reconstruction matrix as conventional reconstruction

method. The reconstructed image had artifact and the pixel counts were significantly overestimated.

Figure 3(d) shows the image reconstructed from truncated projection data using the small FOV detector with high resolution. The projection data were reconstructed by proposed reconstruction method. In the small ROI, the clear image with high resolution was obtained without the artifact and the overestimation, and was almost equivalent to the image from the large FOV detector with high resolution.

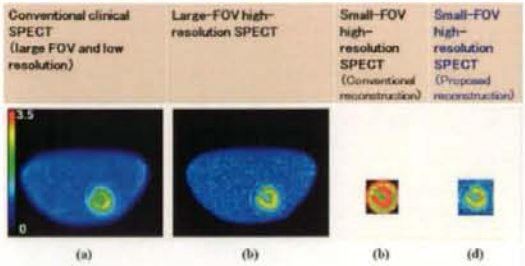

Fig. 3. The reconstructed images obtained in this simulation. All images were displayed with the range of same gray scale [0-3.5] (a) The image obtained from the untruncated projection data of large FOV detector with low resolution as conventional clinical SPECT. (b) The image obtained from the untruncated projection data of large FOV detector with high resolution as the reference image. (c) The image reconstructed from the truncated projection data by small FOV detector with high resolution, on the small reconstruction matrix as conventional reconstruction method. (d) The image reconstructed from the truncated projection data of small FOV detector with high resolution, by proposed reconstruction method.

Figure 4 shows the line profiles in a small ROI on the images obtained from the high-resolution detectors. When the truncated projection data from small FOV detector were reconstructed on the small reconstruction matrix, the obtained image had extremely high counts on the edge of ROI and the pixel counts were wholly overestimated. On the other hand, when the truncated projection data from small FOV detector were reconstructed by our proposed method, the profile of the image had good agreement with that of the image from the untruncated projection data.

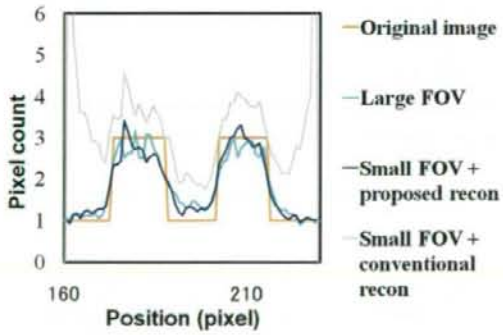

Fig. 4. In a small ROI, the line profiles on the image obtained by reconstructing data from high-resolution detector by each method.

Figure 5 shows the images obtained from projection data acquired by various rotating angles. The image by rotating angle of 150° was almost equivalent to that by rotating angle of 180°. However, the shapes of the hearts were distorted in the images by the rotating angles less than 120°. Usability of the rotating angle of 150° was suggested instead of 180°

Fig. 5. The images reconstructed from projection data acquired by various rotating angles. When the rotating angle is smaller, the radius of rotation can be smaller.

IV. Conclusion

These results suggested feasibility of the combination of two kinds of detectors with small and large FOVs quantitatively obtain high resolution image of a selected small ROI with clinical SPECT. In other words, the image in a selected small ROI can be reconstructed with high resolution and without the effect of truncation by using untruncated data from the large FOV detector, which do not need to have high resolution, even if ROI in small FOV detector with high resolution does not contain the area outside the object.

References

[1] S. R. Meikle, P. Kench, M. Kassiou, and R. B. Banati, "Small animal SPECT and its place in the matrix of molecular imaging technologies," *Phys. Med. Biol.*, vol. 50, no. 22, pp. R45-R61, 2005.

[2] M. Defrise, F. Noo, R. Clackdoyle, and H. Kudo, "Truncated Hilbert transform and image reconstruction from limited tomographic data," *Inverse Problems*, vol. 22, no. 3, pp. 1037-1053, 2006.

[3] L. A. Shepp and Y. Vardi, "Maximum likelihood reconstruction for emission tomography," *IEEE Trans. Med. Imaging*, vol. 1, no. 2, pp. 113-122, 1982.

[4] H. M. Hudson and R. S. Larkin, "Accelerated image reconstruction using ordered subsets of projection data," *IEEE Trans. Med. Imaging*, vol. 13, no. 4, pp. 601-609, 1994.